Progressive pulse dynamics in a mode-locked fiber laser

NI FENG,[1,2] HUI HU[1,2], SEN WANG[1,2], RENLAI ZHOU[1,2,*], AND K. NAKKEERAN[3]

[1]*Key Laboratory of In-Fiber Integrated Optics, Ministry Education of China, Harbin Engineering University, Harbin 150001, China*
[2]*College of Physics and Optoelectronic Engineering, Harbin Engineering University, Harbin 150001, China*
[3]*School of Engineering, Fraser Noble Building, University of Aberdeen, Aberdeen AB24 3UE, UK*
**zhourl@hrbeu.edu.cn*

Abstract: Triple different operation regimes like passive Q-switched (PQS), Q-switched mode-locking (QSML) and continuous-wave mode-locking (CWML) are experimentally observed as progressive pulse dynamics in a mode-locked fiber laser, which is constructed with several-meters of cascaded small-core erbium/bismuth co-doped fiber (EBCF) to engineer the cavity loss modulation. The pulse fission evolution from PQS to QSML to CWML operation is flexibly achieved through pump power variation as the only control parameter at fixed polarization orientation. Output characteristics in all triple operation regimes are studied in detail and particularly the pulse transitional process between PQS and QSML is reported experimentally for the first time, to the best of our knowledge. The laser pulse formation criteria for different operation regimes are also theoretically analyzed. The obtained results and analysis disclose the complete pulses evolution process from PQS to QSML to CWML operation, which contribute to further understanding of the complex nonlinear dynamics and laser pulse formation mechanism in a passively mode-locked fiber laser.

© 2023 Optica Publishing Group under the terms of the Optica Publishing Group Open Access Publishing Agreement

1. Introduction

Mode-locked fiber lasers have attracted much attention due to their high-power density, ultrashort interaction time, and flexible pulse modulation, which are widely applied in micro-processing [1], biomedical diagnosis [2], molecular spectroscopy [3], optical communication [4], and data storage [5], etc. In fiber lasers, a saturable absorber (SA) is included in the resonant cavity to establish mode-locking operation. Based on their material property, the SAs can be categorized into either natural SA materials or effect of saturable absorption created through nonlinear optical devices. For physical SAs, low-dimensional materials are extensively utilized in mode-locked fiber lasers. However, the low-dimensional materials may suffer irreversible damage cause of higher-power laser operation for prolonged time, resulting in increased loss or even failure to achieve the mode-locking operation. Commonly used optical devices to create saturable absorption effect are nonlinear optical loop mirror or amplification loop mirror (NOLM/NALM) [6-8], nonlinear multimode interference (NMI) [9,10], and nonlinear polarization rotation effect (NPR) [11-12]. In NOLM/NALM based fiber lasers, the nonlinear phase shift difference is accumulated by the two optical signals propagated in opposite directions [6]. Nevertheless, in these type of fiber lasers, the threshold power level to self-start mode-locking operation is relatively high, and some additional actions are to be followed to trigger the mode-locking operation. NMI mode-locking makes use of the interference between various modes with different nonlinear phase shifts in a multimode fiber [9]. In NMI based fiber lasers, modulation depth can be controlled by changing the length of the multimode fiber, which is practically inconvenient. NPR mode-locking is based on the variation of polarization state related to the intensity of the optical signal in the cavity, and in which, saturable absorption is achieved by polarizers [12]. Due to the intrinsic advantages of simple structure, high modulation depth, short response time, and low component cost, NPR technique is widely investigated and applied in various fields.

For fiber lasers can be divided into three different pulse operation regimes: passive Q-switched (PQS), Q-switched mode-locking (QSML), and continuous-wave mode-locking (CWML). PQS operation is an outcome of the cavity Q-factor modulation by reiteratively emptying and replenishing the stored cavity energy, while CWML operation results from a fixed phase relation between numerous oscillating longitudinal modes in the cavity. QSML is a special type of operation in which the laser pulses consist of mode-locked pulses on and above a Q-switched envelope. To date, the aforementioned PQS [13,14], QSML [15,16], and CWML [7-12] operations are successfully demonstrated in mode-locked fiber lasers. As a vigorous method to achieve Q-switched or mode-locked operation, various low-dimensional SA materials are utilized as modulating devices to generate the laser pulses. Common materials are graphene [17,18], semiconductor saturable absorption mirrors (SESAMs) [19,20], carbon nanotubes (CNTs) [21,22], transition metal dichalcogenides (TMDs) [23,24], topological insulators (TIs) [25], black phosphorus (BP) [26], Mxenes [27], Xenes [28], phosphorene [29,30], ferromagnetic insulators (FIs) [31,32], silicene [33,34], and tellurene [35]. Mid-Infrared PQS and mode-locked fiber lasers at 2-3 μm wavelength range were demonstrated by incorporating CNT/SESAM/Selenide-nanoflowers SAs in the cavity [14,36, 37]. Also, Q-switched, mode-locked, or continuous-wave (CW) operation was experimentally demonstrated in an Yb-doped double-clad NPR mode-locked fiber laser [38], but the output results were not explicit, and the different operation regimes could not be flexibly switched with a fixed polarization state. Multimode PQS and spatiotemporal mode-locked operation were observed in a multimode fiber laser through specific spatial coupling and half-wave plate (HWP) / quarter-wave plate (QWP) polarizers setup [39]. However, majority of the research investigations focuses on the output pulse characteristics in various operating regimes or synthesizing of new materials for SAs. Seldom research works are conducted in mode-locked fiber lasers to investigate the feasibility for progressive pulse evolution dynamics from PQS to QSML to CWML state, and thorough analysis of the related temporal and spectral transition characteristics between different operation regimes.

In this paper, we propose a cascaded gain-fiber mode-locked laser, and experimentally report the progressive evolution of laser pulses from PQS to QSML to CWML state that is simply achieved through pump power variation as the only control parameter at fixed polarization orientation. The temporal and spectral transition processes from PQS to QSML to CWML operation are recorded and reconstructed, and the laser output properties are analyzed in detail for all three operation regimes. The progressive pulse splitting process from PQS to QSML operation is experimentally demonstrated for the first time, and the built-in loss modulation resulting from the combined effects of the cascaded small-core erbium/bismuth co-doped fiber (EBCF) and the polarization controllers in the cavity is studied. Experimental results and analyses reported in this work can contribute to further comprehending the nonlinear dynamics of passively mode-locked fiber laser.

2. Experimental setup

To study the output performance of pulse laser at various operation regimes, a ring mode-locked fiber laser is constructed as shown in Fig. 1. A 980 nm laser diode (LD) with a maximum pump power of 600 mW is launched into the fiber cavity through a 980/1550 nm wavelength-division-multiplexer (WDM). A 2 m long erbium-doped fiber (EDF) and an 8 m long bismuth-EDF (BEDF) with a core diameter of 4 μm are cascaded as gain media. A polarization-dependent isolator (PD-ISO) is placed between the two polarization controllers (PCs) to ensure unidirectional operation and serves as a polarizer in the laser cavity. PC1 and

PC2 are used to control the polarization state of the light signal in the cavity, that acts as a SA effect creating device together with the PD-ISO to achieve the mode-locking operation. When the light signal propagates in the cavity, both the orthogonal polarization components will accumulate the nonlinear phase shift that are dependent on the light intensity due to the nonlinear Kerr effect. Adjusting the polarization devices gets the head and tail ends of the pulse with lower intensity attenuated to temporally narrow down the pulse width. This narrowing of the pulse continues until gain-loss balance is established, and thus the mode-locked pulses are produced in the cavity. The total length of the cavity is about 14.1 m, which is consists of 10 m long gain fiber (EDF and BEDF) and about 4.1 m long standard single-mode fiber (SMF). Due to core diameter mismatch between BEDF and SMF, fused biconical taper technique was adopted to minimize the splicing loss, and the coupling efficiency was about 84.23%. Laser pulse-train is extracted from the cavity through a fiber output coupler (OC) with 10% ratio. The temporal pulse sequence and output spectrum are measured using a real-time scanning oscilloscope (MSO64, Tektronix) and a spectrum analyzer (AQ6370D) with a resolution of 0.02 nm, respectively. A radio frequency (RF) signal analyzer (FSV-40) with a bandwidth of 10 Hz-40 GHz is used to monitor the repetition rate of the laser output. The autocorrelation trace of the mode-locked pulse is analyzed by a an autocorrelator, and the average output power is measured by a power meter (S470C, Thorlabs) with a wavelength range of 250 nm-10.6 μm.

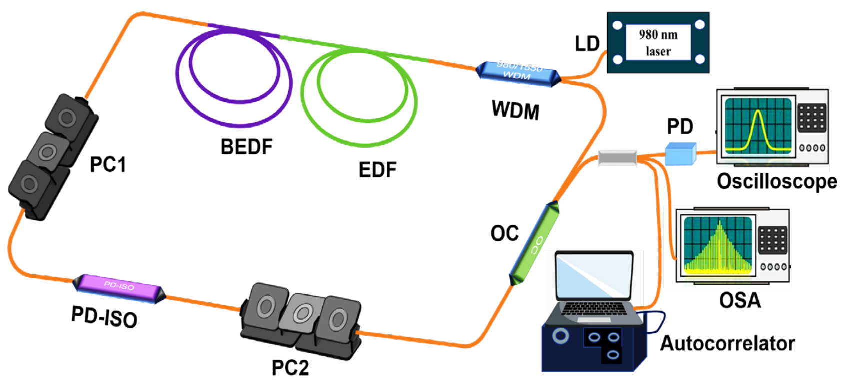

Fig. 1. Experimental setup of the cascaded gain-fiber mode-locked laser. PD: photodiode; OSA: optical spectrum analyzer.

3. Experimental results and discussion

3.1 PQS operation

To initiate a stable PQS operation, the cavity energy needs to be accumulated to a certain value by increasing the pump power and then the cavity loss is sharply reduced by fine adjustments of the PCs. PQS operation of the fiber laser is easily achieved by increasing the pump power to 60 mW. As a single laser operation regime, the PQS state can sustain at pump power ranging from 60 to 200 mW. Figure 2(a) depicts the pulse evolution of the PQS laser output for gradual increase of the pump power in steps of 5 mW. Note that the time interval between adjacent pulses nonlinearly decreases with increase of the pump power, that indicates the increase of pulse repetition rate in accordance to pump power increase (typical feature of PQS operation). In contrast to the previously reported results for the SA-materials-based fiber lasers [35,37], in this experiment the pulse intensity is gradually enhanced as the pump power is increased, which is shown as the bright intensity color in Fig. 2(a). Oscilloscope trace of the pulse-train at 200 mW pump power is shown as blue curve in Fig. 2(a). The profile of the pulse-train is quite uniform without any disturbances or noises indicated that the PQS mode of operation of this laser is highly stable.

Fig. 2(b) shows the evolution of output spectra against various pump power. Spectral profiles are almost similar at different pump power levels, but several peaks appear at fluctuating wavelength locations in the spectrum. In the upper part of Fig. 2(b) the blue and red curves are the output spectra at the pump powers of 105 mW and 120 mW, respectively. The central wavelength of these spectra coincides and located at 1548.06 nm with a 3-dB bandwidth of 5.81 nm. Three distinct peaks contributed by the CW components are observed in the spectrum, and their locations and/or intensities are controllable through the PC orientation maneuver. Figure 2(c) exhibits the pulse repetition rate (blue) and pulse duration (red) versus the pump power levels for a fixed intracavity polarization. The pulse repetition rate linearly rises from 40.54 to 85.42 kHz with a slope of ~3.08 kHz/10 mW, when the pump power is increased from 60 to 200 mW. On the other hand, the pulse duration evolution showed an inversely proportional characteristics with the pump power levels and reduced from 5.88 to 2.55 μs. This can be attributed to the rapid accumulation of intracavity energy at a higher pump power that can swiftly accomplish the transition process between energy emptying and replenishing, which eventually results in a higher repetition rate and shorter duration PQS pulse formation. The average pulse energy and peak power as a function of pump power is shown in Fig. 2(d). The maximum pulse energy of 6.47 nJ is obtained at the pump power of 200 mW, corresponding to a peak power of 2.51 mW.

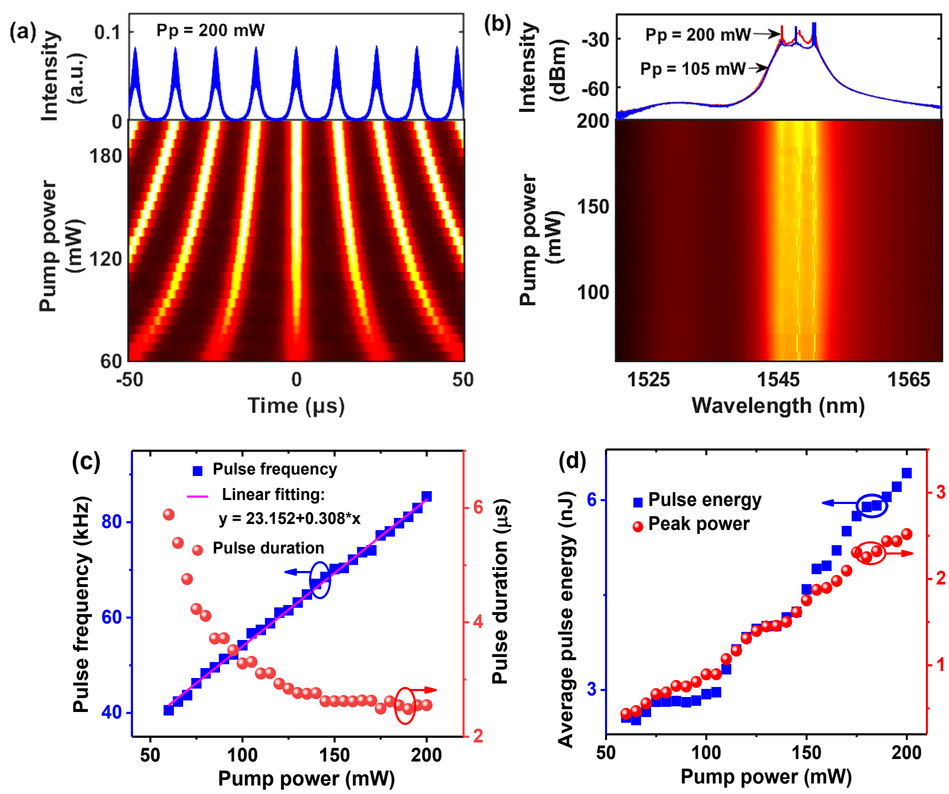

Fig. 2. Output characteristics of PQS pulse laser with pump power ranging from 60 to 200 mW: (a) Evolution of temporal pulses train; (b) Corresponding evolution of output spectra; (c), (d) Pulse repetition rate, pulse duration, average pulse energy and peak power with the pump power increase.

3.2 QSML operation and transition process between PQS and QSML

When the pump power is more than 200 mW, the PQS pulse becomes unstable and the cavity dynamics enters the Q-switched mode-locking (QSML) operation, where the pulses gradually split and the temporal profile of the pulse train is modulated by a periodic Q-switched pulse envelope. Figure 3(a) shows the pulse evolution of QSML laser operation for the pump power ranging from 200 to 300 mW. Time interval between adjacent Q-switched pulse envelopes decreases with increase of pump power, implying the generation of high repetition rate Q-switched pulse envelope as the pump power is increased. Unlike the pulse characteristics in the PQS state, the Q-switched pulse envelope intensity is not enhanced as the pump power is increased, and rather the external pump energy is transferred to the mode-locked pulses in QSML operation. Figure 3(b) displays the zoomed-in view of the pulse evolution of QSML laser for a time range of 2 μs, corresponding to the red-dashed region in Fig. 3(a). Stable mode-locked pulse is gradually formed through a complex evolution process, and the explicit process and formation mechanism are analyzed further in detail later with the results reported in Fig. 4. The spectral evolution of the QSML operation is exhibited in Fig. 3(c), whose central wavelength is located at 1548.11 nm with a 3-dB bandwidth of 5.88 nm. The spectral bandwidth and central wavelength have no obvious change for pump power variations, indicating that the QSML operation has excellent long-term stability.

Zoomed-in view of single Q-switched pulse envelope at a pump power of 280 mW is presented in Fig. 3(d) in blue color, and a screenshot of the pulse sequence over a time range of 100 μs is in yellow color. Mode-locked pulse train is modulated by a Q-switching pulse envelope, and the pulse interval is about 68.9 ns that corresponds to the cavity roundtrip time. The Q-switched pulse envelope is curve fitted by follow function [40]:

$$P(t) = \frac{a}{[\exp(1.76 \times t / t_1) + \exp(-1.76 \times t / t_2)]^2} \qquad (1)$$

where a is the scaling factor, the estimated t_1 =3.87 μs and t_2 =3.70 μs represent the rise-time and fall-time of the Q-switched pulse envelope respectively, and the full width at half maximum (FWHM) of the Q-switched pulse envelope is calculated as $\tau = (t_1+t_2)/2$. In Fig. 3(d), red curve fits well with the Q-switched pulse envelope, the repetition rate of the Q-switched pulse envelope is ~112.57 kHz, and the FWHM of the pulse envelope is ~3.79 μs.

To further investigate the QSML operation, the radio-frequency (RF) spectral distributions are studied for various pump powers and the results are depicted in Fig. 3(e). A central frequency peak accompanied by a series of sideband frequency components are observed, and the frequency of central peak located at about 14.52 MHz (coincides with the fundamental repetition rate of the mode-locked pulse) with a signal-to-noise ratio (SNR) of 59.12 dB. For a fixed pump power, note the uniform frequency interval between adjacent sideband components, which corresponds to the repetition rate of the Q-switched pulse envelope [43]. As noticed in the zoomed-in view of the dashed region in Fig. 3(e), the frequency offset between the adjacent side frequency components shifts farther away from the central frequency while the pump power is increased, and the explicit frequency offsets are measured as 85.42, 106.01, 112.57, and 116.41 kHz for the pump powers of 200, 260, 280 and 300 mW, respectively. Fig. 3(f) shows the variations of the pulse envelope repetition rate, the FWHM of the pulse envelope, and the SNR of the central frequency as a function of the pump power. As the pump power increased from 200 to 300 mW, the pulse envelope repetition rate linearly increased from 85.42 to 116.41 kHz with a slope of 3.47 kHz/10 mW, the FWHM of the pulse envelope is gradually broadened from 2.55 to 5.24 μs nonlinearly, and the SNR of central frequency is improved from 35.84 to 57.11 dB.

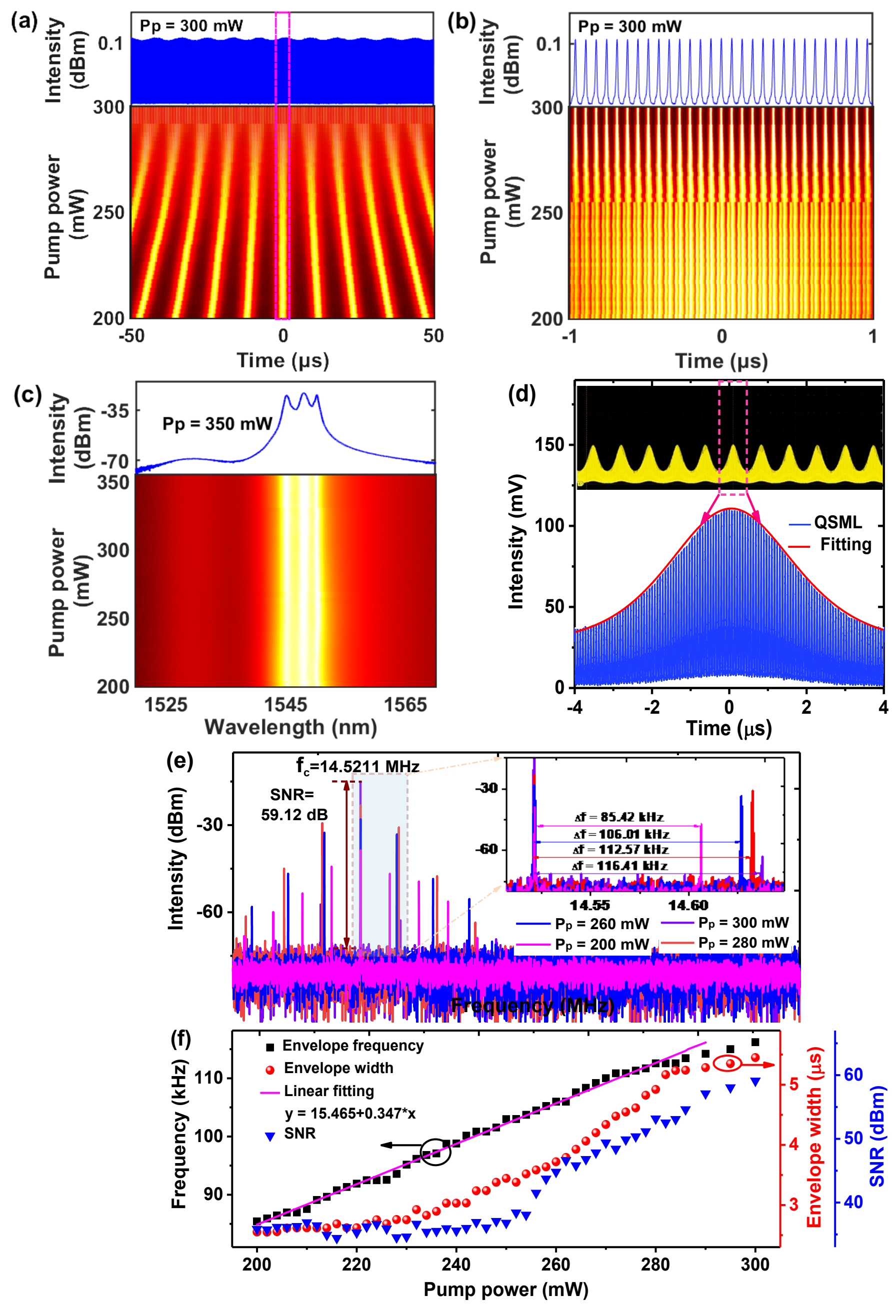

Fig. 3. Properties of QSML pulse laser at different pump powers: (a) Evolution of temporal pulses train, and (b) enlarged view of the dashed region; (c) Evolution of output spectra; (d) Details of a single pulse envelope at the pump power of 280 mW; (e) RF spectra at different pump powers, and the illustration is the enlarged view of the dashed region; (e) Variations of the pulse envelope repetition rate, FWHM of the pulse envelope and SNR of central frequency versus pump power.

To explore the pulse evolution process from PQS to QSML operation, by maintaining the PC orientation fixed, we recorded oscilloscope traces of the output laser pulse train for various pump powers, and the results are exhibited in Fig. 4(a). Figure 4(b) is the zoomed-in view of the pulse trains between -0.9 and 0.9 μs, which corresponds to the dashed region in

Fig. 4(a). PQS pulse starts to break up when the pump power is 180 mW, weak multiple peaks are formed in Q-switched pulse envelope, and the pulse intensity becomes unstable. These dynamics got aggravated as the pump power is further increased, and the modulation depth increased. A double-humped type pulse can be observed in Fig. 4(b), and this type of laser pulse is sustained for the pump power ranging from 180 to 250 mW. When the pump power is increased up to 254 mW, the double-humped peaks begin to merge together into single peak laser pulse, and a stable uniform mode-locked pulse is eventually generated for a pump power of 280 mW. The switching between PQS and QSML operation can be attributed to the built-in loss modulation of the cavity [42-44]. In our experiment, the loss modulation mainly resulted from the combined effects of the PCs and the cascaded small-core EBCF. The several meters small-core EBCF introduces an additive birefringence in the cavity for intensity-dependent phase delay, the laser pulses at different pump powers will undergo different phase delays during intracavity round-trips, which provides the required appropriate conditions to initiate and sustain a stable QSML operation. In addition, a nonlinear phase change is feasibly generated when the laser pulse propagates in EBCF with a 4 μm core diameter, which is beneficial for the formation of intensity-dependent loss modulation in the cavity [42]. If the small-core EBCF is removed from the cavity, the aforementioned evolution process between PQS and QSML state could not be achieved only with the adjustments of the PCs orientation.

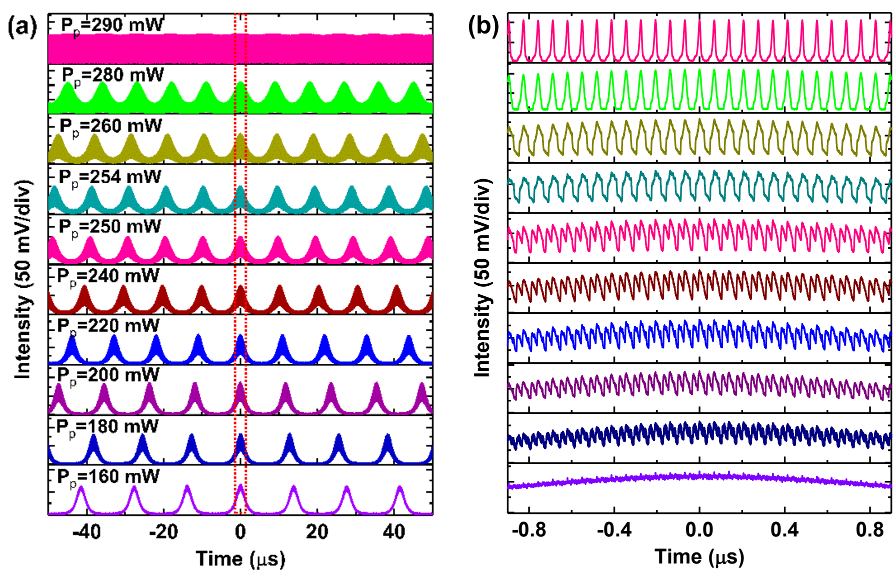

Fig. 4. The pulse evolution process from PQS to QSML state along with the pump power increase: (a) The recorded oscilloscope traces of the pulse train at different pump powers; (b) the zoomed-in view of the pulse train in a time range of 1.8 μs.

3.3 CWML operation

Mode-locking operation is a combined effect of dispersion, nonlinearity, gain, and loss in the cavity. The pump power should be high enough to provide sufficient gain and nonlinearity in the cavity, the weak longitudinal modes are attenuated by the nonlinear saturable absorption effect, while the longitudinal modes with a certain intensity are to be superimposed in-phase, resulting in the mode-locking operation. With a fixed PC orientation, the CWML operation is easily achieved for a pump power of 290 mW. Figure 5 (a) depicts the recorded oscilloscope traces of the pulse trains at 290, 310, 330, and 350 mW pump power over a time range of 100 μs, and the temporal profiles of the pulse trains are maintained with high stability. To show the intensity fluctuation of mode-locked pulse train, the zoomed-in view of the dashed region in Fig. 5(a) is shown in blue as the oscilloscope traces. Weak intensity modulation still exists in the CWML pulse train, and the time interval between adjacent pulse envelopes decreases slightly from ~8.72 to ~8.17 μs for rise in the pump power from 290 to 330 mW, and cease to appear for a pump power of 350 mW. The corresponding RF spectra are exhibited in Fig. 5(b) with a resolution bandwidth (RBW) of 100 Hz and a span of 1.4 MHz. The measured SNRs are 43.25, 48.51, 51.82, and 60.15 dB, indicating that the mode-locking can stably operate in the pump power ranging from 290 to 350 mW. The sideband frequency components are observed in the RF spectra, with frequency offsets of 114.61, 118.91, and 122.41 kHz which corresponds to the time intervals between adjacent pulse envelopes in Fig. 5(a). No sidebands indicate the disappearance of intensity modulation in the pulse train, which is ascertained by the pulse oscilloscope traces at 350 mW pump power. Figure 5(c) depicts the output spectra produced by the CWML laser for various pump powers. The central wavelength is 1547.95 nm with a 3-dB spectral bandwidth of 5.83 nm. It is evident that three wavelength peaks located at 1545.08, 1547.95, and 1550.13 nm are distinct in the spectrum which is caused by the intracavity birefringence-induced spectral filtering effect. The measured intensity autocorrelation trace is shown in Fig. 5(d), and the pulse durations are about 436.81, 415.15, 387.24, and 382.46 fs, and the time-bandwidth products (TBP) are estimated to be 0.22, 0.21, 0.19, and 0.19, which are nearly the transform-limited soliton pulses.

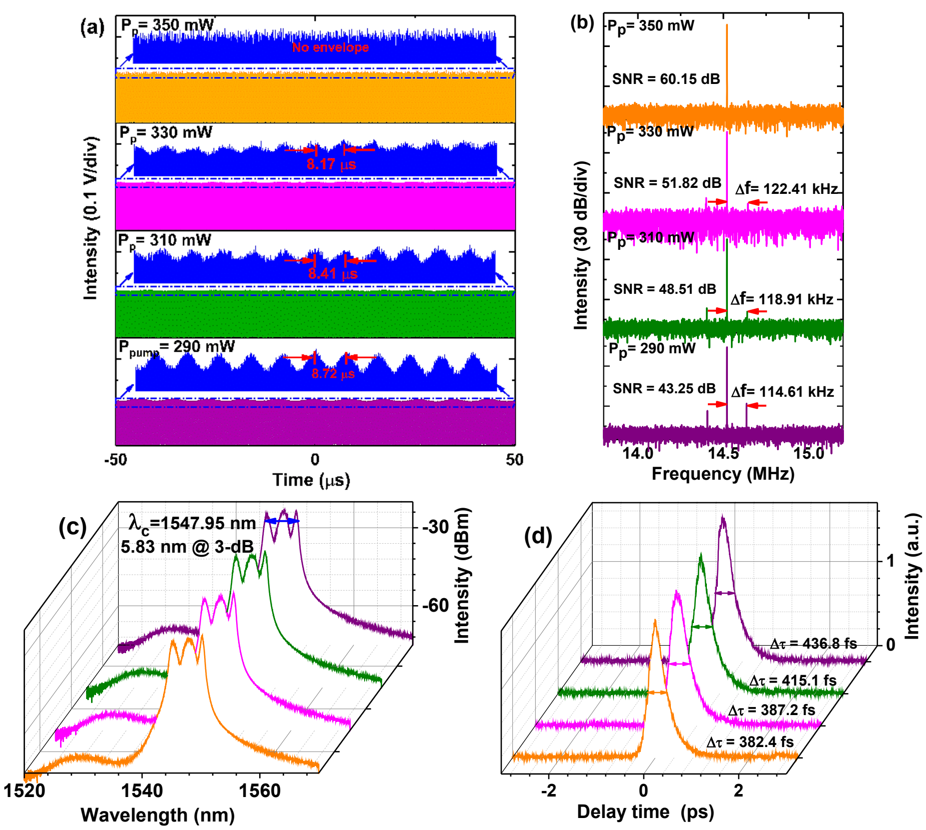

Fig. 5. Properties of CWML pulse laser with pump power ranging from 290 to 350 mW: (a) Temporal pulses train at different pump powers; (b) RF spectra, (c) Mode-locked spectra at different pump powers; (d) Corresponding autocorrelation traces of laser pulses.

4. Discussion

Pulsed fiber laser operation in different regimes such as PQS, QSML, and CWML is dependent on several cavity parameters for instance gain saturation power, gain relaxation time, modulation depth, and saturation power of SA etc. [14-37]. Inclusion of several-meters of small-core EBCF to enhance the built-in loss modulation in the cavity, made our proposed fiber laser dynamics to progressively evolve the lasing signal from PQS to QSML to CWML operation by simply varying the pump power for a fixed cavity polarization. The length of EBCF and/or polarization orientation are found to be additional control features for the laser state operation (similar to diode-pumped solid-state lasers [40]). In the experiment, when the pump power is increased up to 60 mW, the SA reaches saturation, and a high transmittance triggers the PQS pulse generation. Intracavity criterion to generate PQS pulses is [45,46]:

$$\left|\frac{dq}{dI}\right| I > \frac{\tau_R}{\tau_{\text{stim}}} \approx r\frac{\tau_R}{\tau_L} \tag{2}$$

where q is the intracavity loss introduced by SA during each roundtrip. I is the pulse intensity. τ_R is the cavity roundtrip time. τ_L is the upper-level lifetime of the gain fiber and $r = 1 + P / P_{sat}$ is the pump parameter. P and P_{sat} are the laser power and the gain saturation power. From inequality (2) we find that if the gain saturation cannot swiftly respond within the loss reduction per roundtrip time, the cavity gain gets higher than the loss, and hence the laser intensity will increase rapidly, resulting in the generation of PQS pulses. Also, longer upper-level lifetime of the erbium-doped fiber (~10 ms) in the laser cavity [47] is favorable for the PQS pulse formation.

The QSML state can be regarded as a phenomenon of the amplitude modulation of mode-locked pulse caused by the instability of Q-switching. For numerous applications requiring uniform pulse energy and repetition rate, instability in Q-switching to be eliminated. When the pump power is increased to 180 mW, the PQS pulse envelope starts to break up, and stable QSML is gradually established for 300 mW pump power through a series of pulse evolution. The CWML formation criterion far from QSML is expressed as [48]:

$$\left|\frac{dq}{dE_P}\right| E_P < r\frac{\tau_R}{\tau_L} = \frac{\tau_R}{\tau_L} + \frac{E_P}{E_{sat}} \tag{3}$$

where E_{sat} is the gain saturation energy. Compared with inequality (2), the laser intensity I is replaced by the pulse energy E_P in inequality (3), since the gain saturation of SA is caused by the mode-locked pulse energy, rather than the average power of pulses [46]. When the intracavity gain saturation rate is faster than that of the SA, the gain saturation will inhibit the continuous enhancement of the Q-switched pulses. At the same time, if the resonator satisfies the mode-locking condition, then the laser can operate in the CWML state. When the intracavity pulse energy is higher than a certain value caused while increasing the pump power, the pulse laser will cease operating in QSML state and switch to operate in CWML state.

The recorded progressive temporal evolution of laser operation from PQS to QSML to CWML is exhibited in Fig. 6(a). When the pump power is increased from 60 mW to 200 mW, the laser stably operates in PQS state with the pulse repetition rate and peak power get increased as with the pump power. When the pump power increased beyond 200 mW, the PQS pulse becomes unstable and gradually evolve into QSML state. Figure 6(b) exhibits an enlarged QSML pulse evolution for a time range of 30 μs (corresponding to the region A in Fig. 6(a)), in which both Q-switched pulse envelope and mode-locked pulses are observed. With further increase in the pump power, the laser is switched from QSML state to CWML state, and a mode-locked pulse evolution in CWML state for a time range of 2.4 μs (corresponding to the region B in Fig. 6(a)) is shown in Fig. 6(c). Here, the cavity operates in a robust mode-locked state without any intensity fluctuations. Different from the reported results in fiber lasers based on low-dimensional SA materials [14-37], the PQS, QSML, and CWML operation states can be flexibly switched simply by varying the pump power for a fixed polarization, and each state operates sturdily. This versatile switchable mode-locked fiber laser can be used as a seed pulse laser for subsequent power amplification, then further studying the luxuriant nonlinear interactions of laser pulses in highly nonlinear materials, such as photonic crystal fibers, nonlinear optical waveguide, and hollow-core fibers.

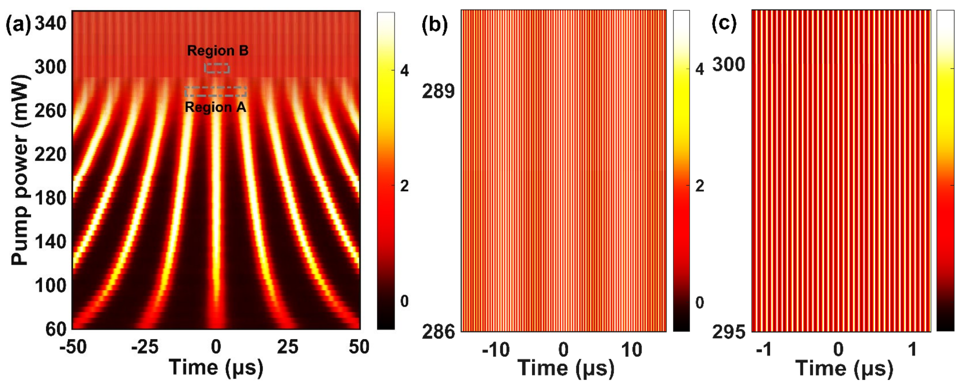

Fig. 6. (a) Progressive temporal evolution of pulse laser from PQS to QSML to CWML state; (b), (c) Zoomed-in pulse evolution in QSML (Region A) and CWML (Region B) operation states.

5. Conclusion

In conclusion, we have experimentally investigated the progressive pulse dynamics in a cascaded gain-fiber mode-locked laser. Due to the intracavity loss modulation resulting from the combined effects of the cascaded small-core EBCF and the polarization controllers, the pulse evolutions from PQS to QSML to CWML state are demonstrated and studied in detail by simply varying the pump power. The small-core EBCF introduces an additional birefringence effect in the cavity for the intensity-dependent phase delay, which provides the necessary conditions to initiate and sustain different operation regimes at suitable pump powers, especially the pulse transitional process between PQS and QSML is experimentally reported for the first time. For PQS state, the repetition rate increases from 40.54 to 85.42 kHz, the pulse duration decreases from 24.66 to 5.88 μs with the increment of the pump power from 60 to 200 mW. For QSML state, the repetition rate of the Q-switched pulse envelope can be linearly tuned from 85.42 to 113.45 kHz with a slope of 3.47 kHz/10 mW, and the FWHM of the Q-switched pulse envelope is gradually increased from 2.55 to 5.24 μs. For CWML state, the center wavelength is 1547.95 nm with a 3-dB bandwidth of 5.83 nm. The fundamental repetition rate is 14.52 MHz with a SNR of >60 dB, which indicates high stability of the generated mode-locked pulses. This research work opens up a novel way of manipulating the operating regimes of mode-locked fiber laser and provides an innovative method to progressively realize the various laser operations from PQS to QSML to CWML state. Moreover, it exposes an effective and realistic technical route to study the complex nonlinear dynamic process in a passively mode-locked fiber laser.

Funding. National Natural Science Foundation of China (62275060).

Disclosures. The authors declare no conflicts of interest.

Data availability. Data underlying the results presented in this paper are not publicly available at this time but may be obtained from the authors upon reasonable request.

References

1. R. R. Gattass and E. Mazur, "Femtosecond laser micromachining in transparent materials," Nat. Photonics **2**(4), 219-225 (2008).
2. A. Ovsianikov, A. Ostendorf, and B. N. Chichkov, "Three-dimensional photofabrication with femtosecond lasers for applications in photonics and biomedicine," Appl. Surf. Sci. **253**(15), 6599-6602 (2007).
3. M. L.Weichman, P. B. Changala, J. Ye, Z. Chen, M. Yan, N. Picqué, "Broadband molecular spectroscopy with optical frequency combs," J. Mol. Spectrosc. **355**, 66-78 (2019).
4. A. Hasegawa, "Soliton-based optical communications: an overview," IEEE J. Sel. Top. Quantum Electron. **6**(6), 1161-1172 (2000).
5. M. Pang, W. He, X. Jiang and P. S. J. Russell, "All-optical bit storage in a fibre laser by optomechanically bound states of solitons," Nat. Photonics, **10**, 454-458 (2016).
6. I. N. Duling, "All-fiber ring soliton laser mode locked with a nonlinear mirror," Opt. Lett. **16**(8), 539-541 (1991).
7. N. Kuse, J. Jiang, C. Lee, T. R. Schibli, M. Fermann, "All polarization-maintaining Er fiber-based optical frequency combs with nonlinear amplifying loop mirror," Opt. Express **24**(3), 3095-3102 (2016).
8. G. Liu, X. Jiang, A. Wang, G. Chang, F. Kaerner and Z. Zhang, "Robust 700 MHz mode-locked Yb:fiber laser with a biased nonlinear amplifying loop mirror," Opt. Express **27**(3), 3518-3527(2019).
9. H. Li, Z. Wang, C. Li, J. Zhang, S. Xu, "Mode-locked Tm fiber laser using SMF-SIMF-GIMF-SMF fiber structure as a saturable absorber," Opt. Express **25**(22), 26546-26553 (2017).
10. J. Lin, Z. Dong, T. Dong, Y. Zhang, C. Dai, P. Yao, L. Xu, "Wavelength switchable all-fiber mode-locked laser based on nonlinear multimode interference," Opt. Laser Technol. **141**, 107093 (2021).
11. J. Szczepanek, T. Kardaś, C. Radzewicz, Y. Stepanenko, "Ultrafast laser mode-locked using nonlinear polarization evolution in polarization maintaining fibers," Opt. Lett. **42**(3), 575-578 (2017).
12. R. Zhou, H. Hu, B. Guo, Q. Li, H. Fu, and K. Nakkeeran, "Self-starting switchable multifunctional solitons fiber laser," Adv. Photonics Res. **3**(5), 2100348 (2022).
13. W. Ma, T. Wang, Q. Su, F. Wang, J. Zhang, C. Wanf, and H. Jiang, "1.9 μm square-wave passively Q-witched mode-locked fiber laser," Opt. Express **26**(10), 12514-12521 (2018).
14. Q. Yi, L. Yang, K. Yang, J. Li, L. Du, B. Huang, Li Miao, and C. Zhao, "Robust nanosecond laser passively Q-switched by tin selenide nanoflowers," Opt. Express **29**(25), 41388-41398 (2021).
15. P. Cheng, Y. Du, M. Han, and X. Shu, "Mode-locked and Q-switched mode-locked fiber laser based on a ferroferric-oxide nanoparticles saturable absorber," Opt. Express **28**(9), 13177-13186 (2020).
16. W. Zhang, G. Wang, F. Xing, Z. Man, F. Zhang, K. Han, S. Fu, "Passively Q-switched and mode-locked erbium-doped fiber lasers based on tellurene nanosheets as saturable absorber," Opt. Express **28**(10), 14729-14739 (2020)
17. Z. Sun, T. Hasan, F. Torrisi, D. Popa, G. Privitera, F. Wang, F. Bonaccorso, D. M. Basko, and A. C. Ferrari, "Graphene mode-locked ultrafast laser," ACS Nano **4**(2), 803-810 (2010).
18. W. Du, H. Li, C. Lan, J. Li, Z. Wang, Y. Liu, "Graphene/WS_2 heterostructure saturable absorbers for ultrashort pulse generation in L-band passively mode-locked fiber lasers," Opt. Express **28**(8), 11514-11523 (2020).
19. S. Tomilov, Y. Wang, M. Hoffmann, J. Heidrich, M. Golling, U. Keller, C. J. Saraceno, "50-W average power Ho:YAG SESAM-mode locked thin-disk oscillator at 2.1 μm," Opt. Express **30**(15), 27662-27673 (2022).
20. Z. Qin, X. Chai, G. Xie, Z. Xu, Y. Zhou, Q. Wu, L. Qian, "Semiconductor saturable absorber mirror in the 3-5 μm mid-infrared region," Opt. Lett. **47**(4), 890-893 (2022).
21. Z. Zhang, Y. Cai, J. Wang, H. Wan, L. Zhang, "Ultrafast stretched-pulse fiber laser mode-locked by carbon nanotubes," Nano Research **3**, 404-411 (2010).
22. L. Dai, Z. Huang, Q. Huang, C. Zhao, A. Rozhin, S. Sergeyev, M. A. Araimi and C. Mou, "Carbon nanotube mode-locked fiber lasers: recent progress and perspectives," Nanophotonics **10**(2), 749-775 (2021).
23. B. Chen, X. Zhang, K. Wu, H. Wang, J. Wang, J. Chen, "Q-switched fiber laser based on transition metal dichalcogenides MoS_2, $MoSe_2$, WS_2, and WSe_2," Opt. Express **23**(20), 26723-26737 (2015).
24. Q. Wu, Z. Wu, Y. Yao, X. Xu, L. Chen, Y. Zhao, K. Xu, "Three-component bright–dark–bright vector pulse fiber laser based on MoS_2 saturable absorber," Opt. Commun. **498**, 127-231 (2021).
25. H. Haris, M. Batumalay, S. J. Tan, A. M. Markom, A. R. Muhammad, S. W. Harun, I. Saad, "Mode-Locked YDFL using topological insulator bismuth selenide nanosheets as the saturable absorber," Crystals **12**(4), 489 (2022).
26. X. Jin, G. Hu, M. Zhang, T. Albrow-Owen, Z. Zheng, T. Hasan, "Environmentally stable black phosphorus saturable absorber for ultrafast laser," Nanophotonics **9**(8), 2445-2449 (2020).
27. C. Ma, W. Huang, Y. Wang, J. Adams, Z. Wang, J. Liu, H. Zhang, "MXene saturable absorber enabled hybrid mode-locking technology: a new routine of advancing femtosecond fiber lasers performance," Nanophotonics **9**(8), 2451-2458 (2020).
28. H. Zhang, S. Sun, X. Shang, B. Guo, X. Li, X. Chen, S. Fu, "Ultrafast photonics applications of emerging 2D-Xenes beyond graphene," Nanophotonics **11**(7), 1261-1284 (2022).

29. Z. Guo, H. Zhang, S. Lu, Z. Wang, S. Tang, J. Shao, P. K. Chu, "From black phosphorus to phosphorene: basic solvent exfoliation, evolution of Raman scattering, and applications to ultrafast photonics," Adv. Functional Materials **25**(45), 6996-7002 (2015).
30. J. He, L.Tao, H. Zhang, B. Zhou, J. Li, "Emerging 2D materials beyond graphene for ultrashort pulse generation in fiber lasers," Nanoscale **11**(6), 2577-2593 (2019).
31. L. Guo, X. Shang, R. Zhao, H. Zhang, D. Li, "Nonlinear optical properties of ferromagnetic insulator $Cr_2Ge_2Te_6$ and its application for demonstrating pulsed fiber laser," Appl. Phys. Express **12**(8), 082006 (2019).
32. R. Sun, L. Guo, X. Shang, H. Zhang, Q. Yue, "Efficient saturable absorber based on ferromagnetic insulator $Cr_2Ge_2Te_6$ in Er-doped mode-locked fiber laser," Nanomaterials **12**(5), 751 (2022).
33. F. Zhang, M. Wang, Z. Wang, K. Han, X. Liu, X. Xu, "Nonlinear absorption properties of silicene nanosheets," Nanotechnology **29**(22), 225701 (2018).
34. G. Liu, J. Yuan, Y. Lyu, T. Wu, Z. Li, M. Zhu, S. Fu, "Few-layer silicene nanosheets as saturable absorber for subpicosecond pulse generation in all-fiber laser," Opt. Laser Technol. **131**, 106397 (2020).
35. W. Zhang, G. Wang, F. Xing, Z. Man, F. Zhang, K. Han, S. Fu, "Passively Q-switched and mode-locked erbium-doped fiber lasers based on tellurene nanosheets as saturable absorber," Opt. Express **28**(10), 14729-14739 (2020).
36. Y. Shen, Y. Wang, H. Chen, K. Luan, M. Tao, and J. Si, "Wavelength-tunable passively mode-locked mid-infrared Er^{3+}-doped ZBLAN fiber laser," Sci. Rep. **7**, 14913 (2017).
37. C. Wei, Y. Lyu, H. Shi, Z. Kang, H. Zhang, G. Qin, and Y. Liu, "Mid-infrared Q-switched and mode-locked fiber lasers at 2.87 μm based on carbon nanotube," IEEE J. Sel. Top. Quantum Electron. **25**(4), 1100206 (2019).
38. A. Hideur, T. Chartier, M. Brunel, M. Salhi, "Mode-lock, Q-switch and CW operation of an Yb-doped double-clad fiber ring laser," Opt. Commun. **198**, 141-146 (2001).
39. K. Liu, X. Xiao, and C. Yang, "Observation of transition between multimode Q-switching and spatiotemporal mode locking," Photon. Res. **9**(4), 530-534 (2021).
40. J. H. Lin, H. R. Chen, H. H. Hsu, M. D. Wei, K. H. Lin, and W. F. Hsieh, "Stable Q-switched mode-locked Nd^{3+}: $LuVO_4$ laser by Cr^{4+}: YAG crystal," Opt. Express **16**(21), 16538-16545 (2008).
41. Y. M. Chang, J. Lee, and J. H. Lee, "A Q-switched, mode-locked fiber laser employing subharmonic cavity modulation," Opt. Express **19**(27), 26627-26633 (2011).
42. J. H. Lin, K. H. Lin, H. H. Hsu, and W. F. Hsieh, "Q-switched and mode-locked pulses generation in Nd: $GdVO_4$ laser with dual loss-modulation mechanism," Laser Phys. Lett. **5**(4), 276-280 (2008).
43. K. H. Lin, J. J. Kang, H. H. Wu, C. K. Lee, and G. R. Lin, "Manipulation of operation states by polarization control in an erbium-doped fiber laser with a hybrid saturable absorber," Opt. Express **17**(6), 4806-4814 (2009).
44. J. Gene, N. H. Park, H. Jeong, S. Y. Choi, F. Rotermund, D. Yeom, and B. Y. Kim, "Optically controlled inline graphene saturable absorber for the manipulation of pulsed fiber laser operation," Opt. Express **24**(19), 21301-21307 (2016).
45. H. A. Haus, "Parameter Ranges for CW Passive Mode Locking," IEEE J. Quantum Electron. **12**(3), 169-176 (1976).
46. F. X. Kartner, L. R. Brovelli, D. Kopf, M. Kamp, I. Calasso, and U. Keller, "Control of solid-state laser dynamics by semiconductor devices," Opt. Eng. **34**(7), 2024-2036 (1995).
47. C. R. Giles, and E. Desurvire, "Modeling erbium-doped fiber amplifiers," J. Lightwave Technol. **9**(2), 271-283 (1991).
48. C. Hönninger, R. Paschotta, F. Morier-Genoud, M. Moser, and U. Keller, "Q-switching stability limits of continuous-wave passive mode locking," J. Opt. Soc. Am. B **16**(1), 46-56 (1999).